ChemMedChem

Chemistry Europe
European Chemical Societies Publishing
ChemMedChem

RESEARCH ARTICLE OPEN ACCESS

Investigating the Inhibitory Properties of Diazo and Pyrazole-Carboxamide-Linked Benzenesulfonamides Against Carbonic Anhydrase Isoforms I, II, IX, and XII

Suleyman Akocak[1] | Nebih Lolak[1] | Andrea Ammara[2] | Gökçenur Gürbüz[3] | Ibrahim Bozgeyik[4] | Demet Taşdemir[5] | Hamada Hashem[6] | Stefan Bräse[7] | Claudiu T. Supuran[2]

[1]Department of Pharmaceutical Chemistry, Faculty of Pharmacy, Adıyaman University, Adıyaman, Türkiye | [2]Dipartimento Neurofarba, Sezione di Scienze Farmaceutiche e Nutraceutiche, Università degli Studi di Firenze, Florence, Italy | [3]Faculty of Pharmacy, Adıyaman University, Adıyaman, Türkiye | [4]Department of Medical Biology, Faculty of Medicine, Adıyaman University, Adıyaman, Türkiye | [5]Department of Medical Biochemistry, Faculty of Medicine, Gaziantep University, Gaziantep, Türkiye | [6]Department of Pharmaceutical Chemistry, Faculty of Pharmacy, Sohag University, Sohag, Egypt | [7]Institute of Biological and Chemical Systems Functional Molecular Systems (IBCS-FMS), Karlsruhe Institute of Technology (KIT), Karlsruhe, Germany

Correspondence: Suleyman Akocak (sakocak@adiyaman.edu.tr) | Claudiu T. Supuran (claudiu.supuran@unifi.it)

Received: 19 February 2026 | **Revised:** 15 June 2026 | **Accepted:** 19 June 2026

Keywords: cancer | carbonic anhydrase | diazo | isoform | pyrazole-carboxamide

ABSTRACT

A novel library of diazo and pyrazole-carboxamide-linked molecules containing the sulfonamide pharmacophore was developed and synthesized, yielding selective inhibitors of clinically relevant carbonic anhydrase (CA) isoforms. The synthesis method involved the production of diazonium salts from 4- and 3-aminobenzenesulfonamide precursors, followed by cyclization and further functionalization to yield structurally diverse pyrazole derivatives. All compounds were evaluated for their inhibitory efficacy against hCA I and II (cytosolic isoforms) and the tumor-associated isoenzymes hCA IX and XII; also, cytotoxicity and molecular modeling studies were conducted for the compounds. The newly synthesized hybrid compounds displayed extensive inhibitory activity, with most derivatives showing significant potency and selectivity for cancer-associated isoforms. More specifically, para-substituted analogs exhibited enhanced inhibitory properties relative to their meta-substituted counterparts. Compound **5f**, with a 3,4-dichloro motif, exhibited the highest activity with a very low K_I value of 1.8 nM against hCA IX, greatly surpassing the reference drug acetazolamide. Electron-withdrawing substituents improved inhibitory efficacy, whereas electron-donating groups often reduced activity. Furthermore, compounds **5f** (A549: 41.17 μM; HCT116: 4.47 μM) and **6c** (A549: 14.64 μM; HCT116: 4.03 μM) showed the lowest IC_{50} values in both cell lines. The findings emphasize diazo- and pyrazole-carboxamide-linked benzenesulfonamides as promising scaffolds for advancing isoform-selective carbonic anhydrase inhibitors.

1 | Introduction

Carbonic anhydrases (CAs; EC 4.2.1.1) make up a ubiquitous family of metalloenzymes, all zinc-dependent, that catalyze the reversible hydration of carbon dioxide (CO_2) to bicarbonate (HCO_3^-) and a proton (H^+) [1–3]. The reaction occurs via a zinc-bound hydroxide nucleophile to maintain homeostasis in acid–base balance, CO_2 transport, and ionic regulation across all domains of life [4]. So far, eight evolutionarily distinct families named α, β, γ, δ, ζ, η, θ, and ι have been characterized and are known in both prokaryotic and eukaryotic organisms [5–7]. Their resemblances include diverged tertiary structures and active-site structures, which are the result of evolution toward specialized biochemical and physiological functions in these families.

In humans, a total of 15 catalytically active and three catalytically inactive carbonic anhydrase-related proteins (CARPs VIII, X, and XI) belong to the α-class of CAs [8–11]. These isoforms are highly diversified with respect to catalytic activity, tissue-specific expression patterns, and subcellular localization, in line with their multidimensional physiological functions [12]. Intracellular pH regulation and metabolic homeostasis are mainly involved with cytosolic isoforms, such as CA I, II, III, VII, and XIII [13, 14]. Conversely, membrane-bound isoforms including CA IV, IX, XII, XIV, and XV promote acid–base balance outside the cell; facilitate the transport of epithelial fluids; and support intercellular communication [15–17]. Because of the mitochondrial isoforms VA and VB, the mitochondrial isoform of CA contributes to the delivery of bicarbonate ions in many vital biosynthetic reactions, especially gluconeogenesis and ureagenesis, indicating its role in the cellular intermediary metabolism [18]. The only secreted isoform is called CA VI, which is localized in salivary releases and has been related to the modulation of sensation, especially taste sensations and natural defense at the oral cavity [19]. Even though CARPs are not active enzymes because they lack the presence of zinc-coordinating histidine residues, it is increasingly becoming evident that they are involved in neurodevelopmental mechanisms and that they may be scaffolding factors or regulate synaptic signaling [20].

Human CAs exhibit structural heterogeneity and compartmentalized distribution, making them targets for pharmacological intervention. Abnormal CA activity has been connected to many pathological processes, such as glaucoma, epilepsy, metabolic alterations such as obesity, and other oncogenic mechanisms [21, 22]. To this end, the rational identification of isoform-selective CA inhibitors has proven to be a beneficial therapeutic approach [23]. The purpose of such inhibitors is to take advantage of isoform-selective differences in active-site architecture and peripheral binding domains and, therefore, increase selectivity and reduce off-target activation [24].

CA IX and XII, membrane-bound isoforms of the carbonic anhydrase enzyme family, exhibit elevated expression levels in malignant tissues [25, 26]. Their upregulation is a hallmark of hypoxic tumor microenvironments and plays a pivotal role in maintaining intracellular pH homeostasis under conditions of intensified metabolic activity [26]. These membrane-associated isoforms function synergistically with the cytosolic carbonic anhydrase variants, particularly CA I and CA II, to neutralize excess proton accumulation resulting from both aerobic and anaerobic glycolytic flux.

The glycolytic metabolism of cancer cells makes excessive amounts of protons (H^+) as metabolic waste products [27]. Protons inside cells combine with bicarbonate ions (HCO_3^-) to make carbonic acid (H_2CO_3), which is then changed into water (H_2O) and carbon dioxide (CO_2) by cytosolic carbonic anhydrases (CAs) (Figure 1). The CO_2 released readily diffuses through the plasma membrane and interacts with the extracellular catalytic domains of membrane-bound carbonic anhydrase isoforms IX and XII, which are often overexpressed in hypoxic tumor microenvironments [28]. These tumor-associated isoenzymes speed up

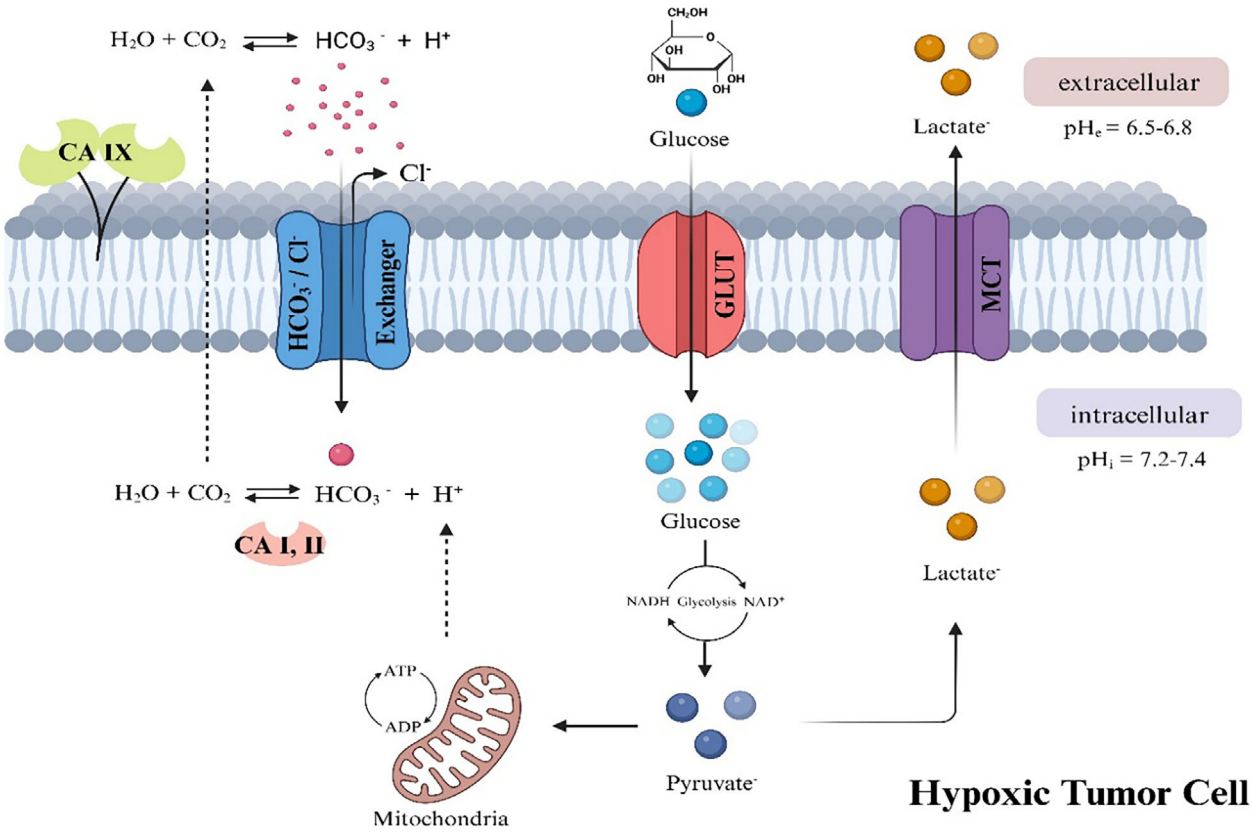

FIGURE 1 | Schematic representation of acidosis in hypoxic tumors due to hypoxia, displaying the increase of glycolysis and the pivotal involvement of carbonic anhydrases in managing intracellular pH and the acidification of the external tumor environment.

the rapid hydration of CO_2, which provides bicarbonate and H^+ ions in the extracellular environment [29]. Chloride/bicarbonate exchangers, especially anion exchanger 2 (AE2), then reabsorb the bicarbonate that was made outside the cell, restoring the cell's ability to buffer. At the same time, an accumulation of H^+ ions outside the cells makes the tumor microenvironment more acidic, which is a sign of aggressive cancer types. The dual regulation of pH enables neoplastic cells to maintain intracellular pH homeostasis during metabolic acidosis, promoting cellular proliferation, inhibiting apoptosis, and enhancing metastatic potential. The characteristics of CA IX and XII in these processes demonstrate their importance as pharmaceutical targets. Targeted inhibition of these isoforms may disrupt pH control, increase tumor cell vulnerability to acidic stress, and prevent tumor development. The design and development of isoform-specific carbonic anhydrase inhibitors signify a viable therapeutic strategy in oncology, particularly within the context of enzyme-targeted drug discovery.

Compounds containing diazenyls, mostly characterized as aromatic azo and diimide derivatives, are characterized by an -N═N-bond between two aromatic or heterocyclic moieties [30–32]. This π-conjugation of a system allows a great deal of electron delocalization, which gives it strong chromogenic properties and allows it to interact with many noncovalent species (e.g., hydrogen bonding and coordination with metal ions). The various pharmacological effects witnessed in this classification, such as antimicrobial, antifungal, antiviral, antidiabetic, and antineoplastic effects, are based on these physicochemical properties [33–36]. The diazenyl sulfonamide analog Prontosil was the first effective antibacterial chemotherapeutic agent in the history of predominantly targeted bacterial infections; its efficacy against streptococcal infections was an incentive to discover sulfa drugs and solidified azo-linked frameworks as working pharmacophores in medicinal chemistry. Recent study evidence indicates that heterocyclic azo dyes are increasingly favored for their dual functionality as an imaging system for drug delivery and as a therapeutic option [37]. They have been effectively exploited as photoresponsive and brightly colored materials to create multifunctional probes for diagnostic and therapeutic applications. Additionally, the aminopyrazole structure has emerged as a prominent heterocyclic framework in pharmaceutical chemistry [38–40]. The remarkable versatility of its architecture, along with its advantageous physicochemical properties, including superior lipophilicity, hydrogen bond formation capability, and metabolic stability, makes it very suitable for drug development.

The pyrazole rings are a significant system in the pharmaceutical research because they provide an influential scaffold, as pyrazoles naturally occur and have been used in various pharmaceutical applications. This type of 5-membered heterocycle has been integrated with several bioactive molecules with antiviral, antitumor, antidepressant, anti-inflammatory, and antioxidant properties [38–47]. Their ability to target a wide range of biological targets makes it very adaptive to regulate various physiological mechanisms. A pyrazole group is often essential to enhance the efficacy of commercial therapeutics and increase the binding affinity and metabolic stability. This trend means that the pyrazoles have been incorporated into medicinal chemistry, especially in the design of molecules that can regulate enzyme activity or receptor occupancy [40, 41]. Compounds derived from aminopyrazole exhibit diverse bioactivities, encompassing antihyperglycemic, anti-inflammatory, antibacterial, antifungal, anticancer, antiviral, antitubercular, and antidiabetic effects [41–44]. Several classes of such substances have demonstrated considerable inhibition of carbonic anhydrase isoforms, indicating possible therapeutic applications in glaucoma, epilepsy, and cancer [45]. The pyrazole ring can be systematically altered to provide precise modifications to target affinity and selectivity, hence facilitating drug discovery and high-throughput screening. A recent study identified aminopyrazoles as ATP-competitive inhibitors of cyclin-dependent kinase 2 (CDK2) in conjunction with Cyclin E, a crucial regulator of the cell cycle [46]. Derivatives of 4-arylazo-3,5-diaminopyrazole have demonstrated promising biochemical properties, positioning them as potential lead compounds in kinase treatments targeting cancer [47].

The suggested diazenyl-layered chromophoric systems coupled with aminopyrazole-pointed structures have become a promising method for the methodical creation of multifunctional pharmaceuticals [48, 49]. It is a hybridization that makes use of the stable pi-conjugation of diazenyl groups/metal-binding properties and the pharmacophoric capacity, as well as the outstanding physicochemical properties of aminopyrazoles [50]. With synthetic accessibility potential, structural plasticity, and bioactivity signatures, they are highly attractive to drug development targeting enzymatic pathways and receptor-mediated pathways. This research synthesizes a novel class of benzenesulfonamides via diazo and pyrazole-carboxamide linkages. The objective of these molecules is to exploit the synergistic effects of sulfonamide-based pharmacophores that exhibit favorable binding to several isoforms of carbonic anhydrase. Initial biological investigations have demonstrated significant and specific inhibitory characteristics, particularly against tumor-associated enzymes hCA IX and XII, hence emphasizing the potential for cancer-related drug development using this scaffold combination.

2 | Results and Discussion

2.1 | Chemistry

Our benzenesulfonamide functionality derivatives with new diazo and pyrazole carboxamide linkages were made using a commandingly refined and reproducible preparation series, as shown in Scheme 1. This procedure is based on a prior reported procedure, which we have improved in our laboratory [51–53]. In brief, the synthesis begins with diazotization of 4,3-aminobenzenesulfonamides (**1a** and **1b**). The resulting diazonium products are then reacted with malononitrile to produce hydrazone intermediates (**3a** and **3b**) that serve as the building blocks in the construction of pyrazole rings. These hydrazones are then cyclized with hydrazine monohydrate to produce pyrazole cores (**4a** and **4b**) in unswervingly good yields in accordance with prior reports [54–59]. These pyrazoles are, in the last step, reacted with substituted isocyanates to give the desired compounds **5(a–f)** and **6(a–f)**. The coloration of the products was intense, which implies that azo coupling was successful. Simple filtration and diethyl ether washing were used to purify and isolate the crude compounds to obtain well-defined materials that could be used in further pharmacological studies.

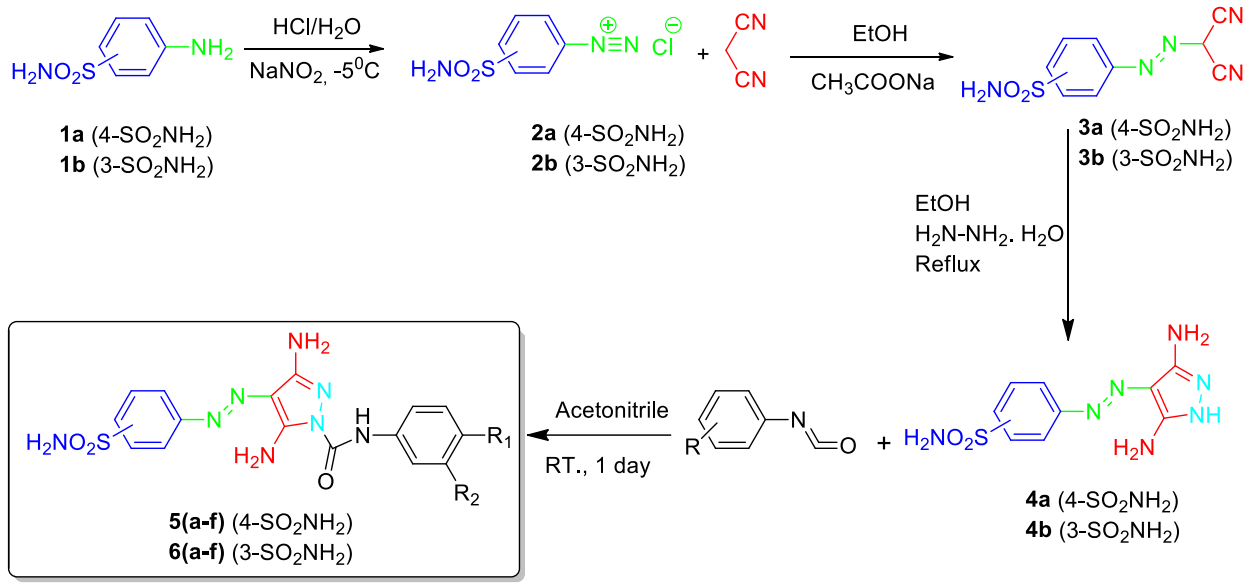

SCHEME 1 | General synthetic procedure of new diazo and pyrazole-carboxamide-linked benzenesulfonamides.

2.2 | Biological Evaluation

2.2.1 | *Carbonic Anhydrase Inhibition Results*

The rational design of novel pyrazole derivatives with enhanced selectivity and potency remains an active field of research due to their clinical significance. Modifying these compounds to inhibit CAs specifically presents promising strategies for treating cancer and other diseases associated with CA isoforms in pathophysiology. The ongoing investigation of pyrazole-derived structures is expected to produce next-generation therapeutics characterized by improved specificity and diminished off-target effects.

The present investigation performed a systematic evaluation of twelve sulfonamide-based compounds **5(a–f)** and **6(a–f)** to determine their inhibitory properties against four representative hCA isoforms: hCA I and II (cytosolic), and hCA IX and XII (tumor-associated transmembrane variants). Acetazolamide (AAZ), a well-known pan-inhibitor of hCAs, was used as a standard to compare both the potency and selectivity of the new derivatives (Table 1).

(i) A detailed structure–activity relationship (SAR) analysis demonstrated that both the spatial orientation of the sulfonamide pharmacophore and the electronic characteristics of substituents at positions R_1 and R_2 substantially influenced inhibitory efficacy. It is important to note that compounds with para-substituted sulfonamide groups **5(a–f)** consistently showed stronger inhibition of all tested isoforms than their meta-substituted counterparts

TABLE 1 | Inhibition data of hCA I, II, IX, and XII with diazo and pyrazole-carboxamide containing compounds **5(a–f)** and **6(a–f)** reported here and the standard sulfonamide inhibitor acetazolamide (AAZ) by a stopped flow CO_2 hydration assay.

				K_I, nM[a]			
Compounds	**SO_2NH_2**	**R_1**	**R_2**	**hCA I**	**hCA II**	**hCA IX**	**hCA XII**
5a	*p*	CH_3	H	1604	50.9	35.0	100.3
5b	*p*	F	H	629.3	26.2	12.1	60.4
5c	*p*	Cl	H	449.3	73.2	28.9	49.1
5d	*p*	H	CH_3	904.2	94.8	24.7	11.6
5e	*p*	H	Cl	684.8	44.0	6.5	15.0
5f	*p*	Cl	Cl	518.3	32.6	1.8	9.3
6a	*m*	CH_3	H	5489	599.3	80.4	148.6
6b	*m*	F	H	6974	627.0	165.5	389.2
6c	*m*	Cl	H	5072	272.8	107.8	205.1
6d	*m*	H	CH_3	9568	417.4	89.2	325.0
6e	*m*	H	Cl	8612	319.6	302.8	219.7
6f	*m*	Cl	Cl	12 100	754.0	413.2	158.7
AAZ	—	—	—	250	12.0	25.0	5.7

[a]Mean from 3 different assays, by a stopped flow technique (errors were in the range of ±5%–10% of the reported values).

6(a–f). This trend is probably due to improved steric compatibility and electronic complementarity with the active site architecture, thereby making binding interactions more favorable.

(ii) Electron-withdrawing substituents, particularly chlorine and fluorine, were positively correlated with inhibitory potency. Compound **5f** ($R_1 = Cl$, $R_2 = Cl$) emerged as one of the most potent derivatives against the tumor-associated isoform hCA IX, exhibiting a K_I value of 1.8 nM, which is substantially lower than that of the reference inhibitor **AAZ** ($K_I = 25.0$ nM). Against hCA XII, compound **5f** also displayed strong inhibitory activity ($K_I = 9.3$ nM); however, it was slightly less potent than **AAZ** ($K_I = 5.7$ nM). Similarly, compound **5e** ($R_1 = H$, $R_2 = Cl$) showed remarkable inhibition of hCA IX with a K_I value of 6.5 nM. Overall, the presence and appropriate positioning of halogen substituents, particularly in the para orientation, appear to contribute favorably to potency and selectivity toward the tumor-associated carbonic anhydrase isoforms. In contrast, derivatives bearing electron-donating methyl groups, such as **5a**, **5d**, and **6d**, generally exhibited reduced inhibitory activity. Compound **5a** ($R_1 = CH_3$, $R_2 = H$) was among the least active members of the para-substituted series, suggesting that methyl substituents may not provide optimal interactions within the enzyme active site.

(iii) Selectivity screenings showed that the majority of the compounds exhibited little activity against hCA I and selectively inhibited the tumor-related hCA IX and hCA XII. Compound **5f** was the strongest hCA IX inhibitor known, which outperforms its reference drug AAZ. Additionally, both compounds **5b** and **5e** were shown to exhibit great efficacy against hCA IX and, at the same time, maintain good selectivity. Among all the meta-substituted analogs, **6a** ($R_1 = CH_3$, $R_2 = H$) and **6d** ($R_1 = H$, $R_2 = CH_3$) were moderately active against hCA IX and XII but were significantly less active against hCA I and II. The following observations contribute to the hypothesis that meta-substitution reduces the performance of binding because of inefficient spatial positioning.

(iv) The SAR data demonstrate that para-substitution is essential to promote an increase in inhibitory potential in the presence of electron-withdrawing groups, in particular, halogens, to oncogenic carbonic anhydrase isoforms. Compound **5f**, which is very specific and potent against specific isoforms, is an ideal starting point for designing new anticancer therapeutics against hCA IX and XII.

2.2.2 | *Cytotoxicity Results*

The MTT assay revealed that the compounds in question decreased the cellular viability in a concentration-dependent fashion. IC_{50} determination of compounds **5c**, **5e**, **5f**, **6a**, **6c**, and **6e** showed strong cytotoxicity of compounds on the two cell lines. The IC_{50} values of these substances ranged between 14.64 and 49.80 μM in an A549 cell line and 3.82 and 14.31 μM in an HCT-116 cell line, thus showing that the induction of cell death was over 50% in both cell lines. Table 2 gathers the data on the IC_{50} of these compounds.

TABLE 2 | IC_{50} (μM) values of the tested compounds in A549 and HCT-116 cell lines as determined by MTT analysis.

	IC_{50}, μM	
	A549	**HCT-116**
5a	66.16	17.53
5b	66.97	17.23
5c	**46.37**	**14.31**
5d	70.55	21.12
5e	**46.24**	**14.26**
5f	**41.17**	**4.47**
6a	**28.99**	**8.52**
6b	81.71	13.77
6c	**14.64**	**4.03**
6d	75.80	4.86
6e	**49.80**	**3.82**
6f	62.16	6.02
SLC-0111	>100	21.12
Cisplatin	>100	>100

Note: The best compounds from the series were shown as a bold for thested 2 cell lines.

In comparative evaluation, several compounds exhibited lower IC_{50} values than the reference compounds. SLC-0111 showed moderate cytotoxic activity in HCT-116 cells ($IC_{50} = 21.12$ μM), while no significant effect was observed in A549 cells ($IC_{50} > 100$ μM). Cisplatin did not exhibit significant cytotoxicity under the tested conditions in either cell line. The lowest IC_{50} values were recorded for compounds **5f** (A549: 41.17 μM; HCT116: 4.47 μM) and **6c** (A549: 14.64 μM; HCT116: 4.03 μM), indicating their status as the most potent cytotoxic agents. The findings suggest that the six compounds were selected to improve practicality, particularly in the HCT116 colorectal carcinoma cell line, and these compounds may serve as viable options for anticancer drug development. Figure 2A–G illustrates the effects of the tested compounds on cell viability in A549 and HCT-116 cell lines.

2.3 | Molecular Docking Study

Molecular docking analysis within the active site of hCA IX reveals a conserved primary anchoring mechanism for all evaluated compounds, driven by the sulfonamide nitrogen establishing a direct coordination bond with the catalytic zinc ion (Zn 264). This metal center is strictly maintained by the canonical histidine triad consisting of His-94, His-96, and His-119 (Figure 3). While the reference inhibitor acetazolamide secures its position through localized hydrogen bonding with Thr-200 and Thr-201 alongside minor hydrophobic contacts with Val-121 and Gln-92, the synthesized pyrazole derivatives (**5d**, **5e**, and **5f**) adopt a significantly more extended

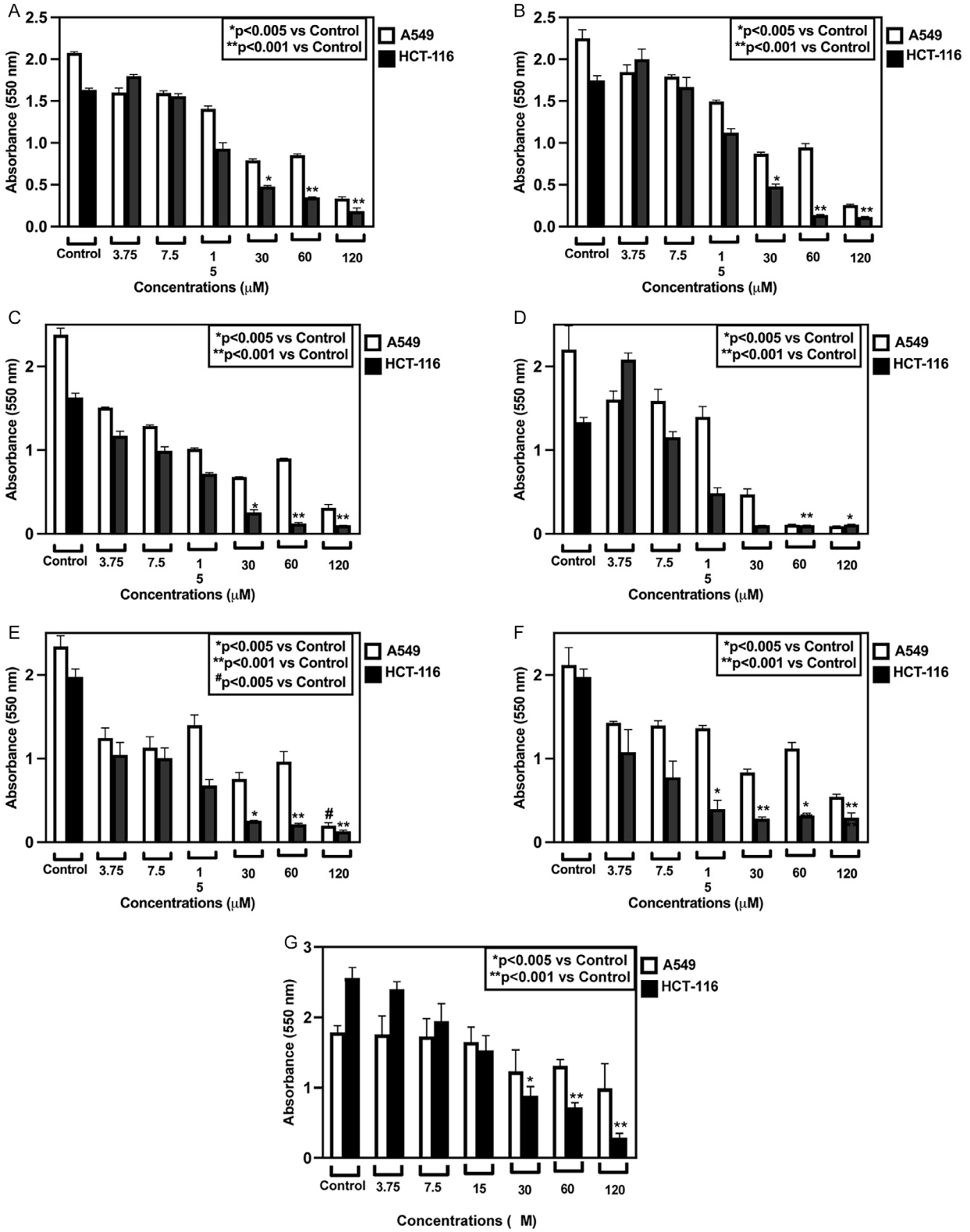

FIGURE 2 | Evaluation of the cytotoxic effects of the selected compounds on A549 and HCT-116 cell lines by MTT analysis. Panels show the cell viability results of compounds (A) **5c**, (B) **5e**, (C) **5f**, (D) **6a**, (E) **6c**, (F) **6e**, and (G) **SLC-0111**, respectively. A significant decrease in cell viability was observed with increasing concentrations, and notably, compounds **5f** and **6c** exhibited the strongest cytotoxic effects in both cell lines. Statistical analysis was performed relative to the control group, where $^{*}p < 0.05$ and $^{**}p < 0.001$ indicate statistically significant differences. Data are presented as mean ± SD ($n = 3$).

conformation within the binding cleft (Figure 3). This structural elongation allows the pyrazole scaffold to maintain the critical hydrogen bonds with Thr-200 and Thr-201 while establishing an additional interaction with Pro-202. More importantly, the extended aromatic system of these derivatives deeply penetrates a neighboring lipophilic pocket, engaging in robust π–π stacking and hydrophobic interactions with Trp-9 and His-68. This extensive engagement of the active site boundaries

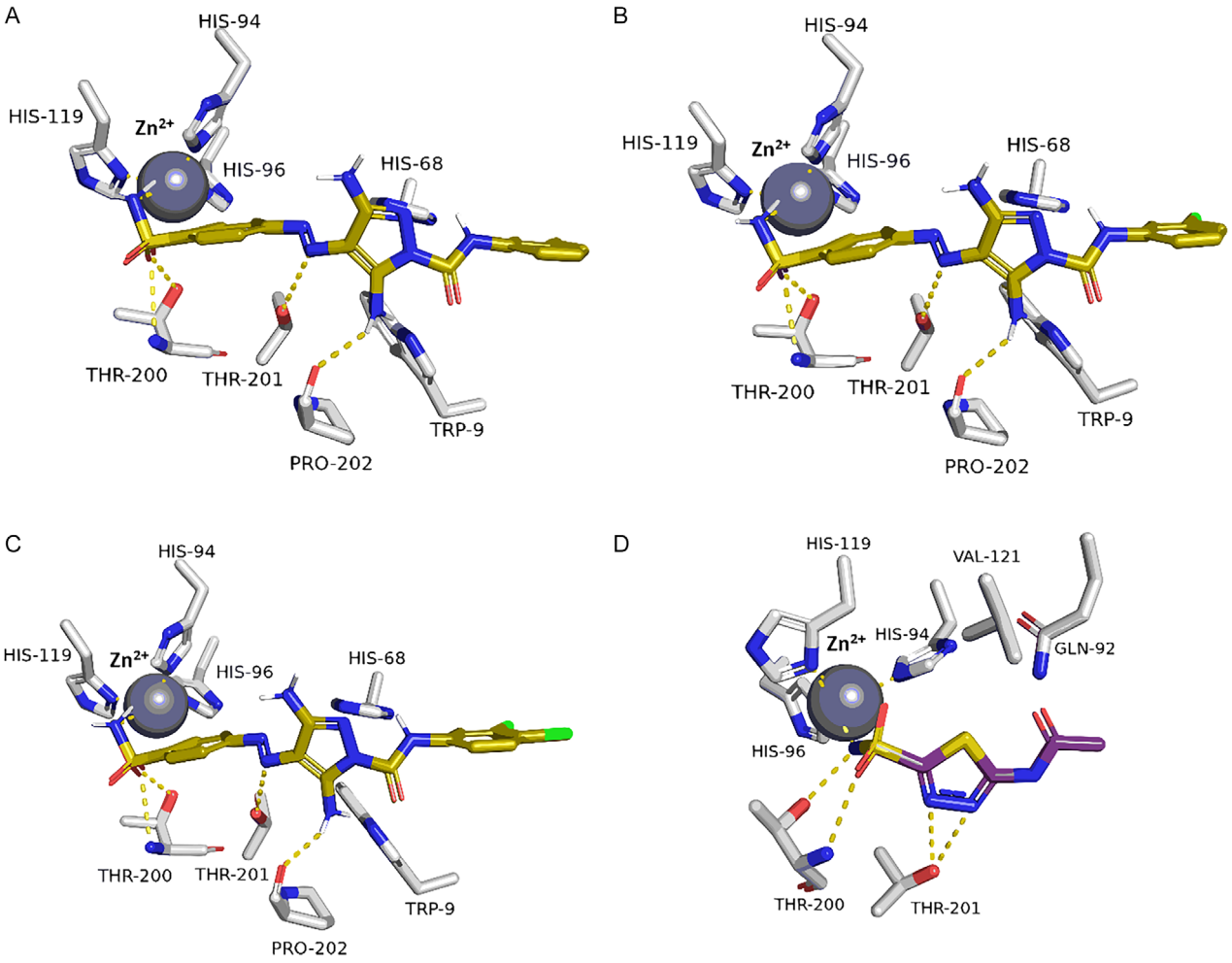

FIGURE 3 | 3D binding poses of the synthesized pyrazole derivatives **5d** (A), **5e** (B), **5f** (C), alongside the reference drug acetazolamide (D), within the active site of hCA IX (PDB ID: 5FL4).

provides a clear structural rationale for the marked enhancement in binding affinities observed for the pyrazole series (−7.72 to −7.74 kcal/mol) relative to acetazolamide (−5.56 kcal/mol) (Table 3).

A parallel structural paradigm dictates the binding behavior within the hCA XII isoform. The primary pharmacophore again acts as a classic metal-acceptor, coordinating the Zn 301 ion, which is stabilized by the localized triad of His-97, His-99, and His-123 (Figure 4). Acetazolamide relies on a dense hydrogen bond network involving Thr-204 and Thr-205, complemented by localized hydrophobic packing against Leu-203. In contrast, compounds **5d**, **5e**, and **5f** project their rigid frameworks across the active site to secure a broader footprint. They anchor via explicit hydrogen bonds with Thr-204 and Ser-139, while the central aromatic features are effectively sandwiched between the aliphatic side chains of Val-125 and Leu-203. This optimal spatial orientation facilitates strong π–alkyl interactions that stabilize the core of the molecules (Figure 4). The transition from the highly localized binding mode of the reference drug to a broader network of distributed polar and π-driven hydrophobic contacts ultimately translates to the superior predicted binding energies of the pyrazole derivatives (−6.43 to −6.57 kcal/mol) compared to acetazolamide (−5.16 kcal/mol) (Table 3).

3 | Conclusions

The current study presents the high potential of a new generation of diazo-pyrazole hybrids incorporating a sulfonamide pharmacophore that is suggested through their rational development and chemical synthesis. It is expected that these compounds will selectively block carbonic anhydrase isoforms in oncogenesis. Derivatives containing a 4-aminobenzenesulfonamide core were always the most active, and para-substituted derivatives the most strongly active. A 3,4-dichloro substitution of the inhibitory constant (K_I) of compound **5f** against hCA IX was established to be 1.8 nM, which is significantly stronger than the reference drug, acetazolamide. It was shown that compound **5e** had strong dual activity as an inhibitor of hCA IX and hCA XII. The SAR analysis showed that the effect of electron-withdrawing substituents significantly increased the inhibitory potency and that the effect of electron-donating substituents reduced the activity; in addition, para-substitutions always performed well in comparison to meta-substitutions. The findings suggest that diazo-pyrazole sulfonamide hybrids serve as an appropriate foundation for the advancement of the subsequent generation of carbonic anhydrase inhibitors. They establish an adequate basis for future research on cancer therapies, encompassing examinations of mechanisms and comprehensive assessments in both in vitro and in vivo settings.

TABLE 3 | Binding energies and interactions of pyrazole derivatives **5d**, **5e**, **5f**, and acetazolamide against hCA IX (PDB ID: 5FL4) and hCA XII (PDB ID: 8CO3).

Compound	Target	Binding affinity, kcal/mol	Amino acid residue/Metal interaction	Type of interaction
AAZ	CA IX	−5.56	-Zn 264	-Metal-acceptor
			-THR 200	-H-bond
			-THR 201	-H-bond
			-VAL 121	-Hydrophobic
			-GLN 92	-Hydrophobic
5d	CA IX	−7.72	-Zn 264	-Metal-acceptor
			-THR 200	-H-bond
			-THR 201	-H-bond
			-PRO 202	-H-bond
			-TRP 9	-π–π stacking
			-HIS 68	-π–π stacking/Hydrophobic
5e	CA IX	−7.65	-Zn 264	-Metal-acceptor
			-THR 200	-H-bond
			-THR 201	-H-bond
			-PRO 202	-H-bond
			-TRP 9	-π–π stacking
			-HIS 68	-π–π stacking/Hydrophobic
5f	CA IX	−7.74	-Zn 264	-Metal-acceptor
			-THR 200	-H-bond
			-THR 201	-H-bond
			-PRO 202	-H-bond
			-TRP 9	-π–π stacking
			-HIS 68	-π–π stacking/Hydrophobic
AAZ	CA XII	−5.16	-Zn 301	-Metal-acceptor
			-THR 204	-H-bond
			-THR 205	-H-bond
			-LEU 203	-Hydrophobic
5d	CA XII	−6.43	-Zn 301	-Metal-acceptor
			-THR 204	-H-bond
			-SER 139	-H-bond
			-VAL 125	-π-Alkyl
			-LEU 203	-π-Alkyl
5e	CA XII	−6.55	-Zn 301	-Metal-acceptor
			-THR 204	-H-bond
			-SER 139	-H-bond
			-VAL 125	-π-Alkyl
			-LEU 203	-π-Alkyl
5f	CA XII	−6.57	-Zn 301	-Metal-acceptor
			-THR 204	-H-bond
			-SER 139	-H-bond
			-VAL 125	-π-Alkyl
			-LEU 203	-π-Alkyl

4 | Materials and Methods

4.1 | Chemistry

4.1.1 | *General Chemical Tecniques*

All chemicals and anhydrous solvents were procured from Sigma–Aldrich, Merck, Alfa Aesar, and TCI, and used without any additional purification. Melting points (mp) were determined using an SMP30 melting point apparatus in open capillaries. FT-IR spectra were recorded using a Perkin Elmer Spectrum 100 FT-IR spectrometer. Nuclear Magnetic Resonance (^{1}H-NMR and ^{13}C-NMR) spectra of the compounds were acquired using a Bruker Advance III 300 MHz spectrometer in DMSO-d_6 with TMS as an internal standard. The ^{1}H-NMR operated at 300 MHz, while the ^{13}C-NMR operated at 75 MHz. Thin-layer chromatography (TLC) was conducted on Merck silica gel 60 F_{254} plates.

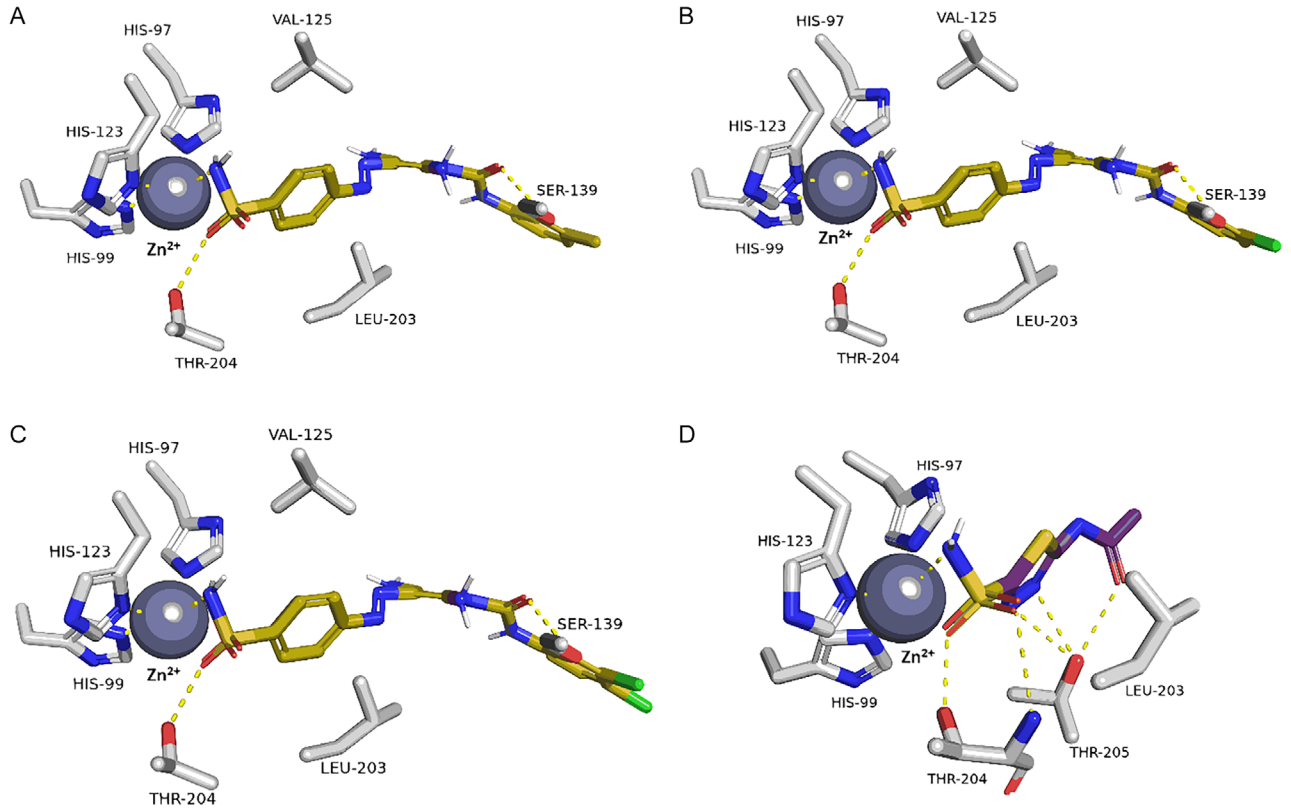

FIGURE 4 | 3D binding interactions of the pyrazole derivatives **5d** (A), **5e** (B), **5f** (C), and acetazolamide (D) localized within the active site of hCA XII (PDB ID: 8CO3).

4.1.2 | *Chemical Synthesis*

4.1.2.1 | *General Synthetic Procedure for the Synthesis of Diazo and Pyrazole-Carboxamide-Linked Benzenesulfonamides 5(a–f) and 6(a–f).* Two sulfonamide-based anilines (sulfanilamide and metanilamide) were transformed into their corresponding diazonium salts and then condensed with malononitrile. The overall strategy followed modified versions of methods previously optimized in our laboratory [51–53]. Briefly, the selected sulfonamide derivative (10 mmol) was suspended in distilled water and acidified with HCl. The mixture was cooled to 0°C–5°C and stirred magnetically until a clear solution was obtained. After 15–20 min of equilibration at this temperature, an ice-cold aqueous solution of sodium nitrite (15 mmol) was added dropwise, maintaining the temperature below 5°C. The formation of the diazonium salt normally took about 30 minutes to be complete. Then, drop by drop, malononitrile (10 mmol) previously dissolved in ethanol was added to the diazonium solution, and constant cooling (5°C) was kept. A saturated solution of sodium acetate was then added gradually at that point to bring the pH to 5–6. After the addition, the reactive mixture was left to equilibrate at ambient temperature for 24 h. The precipitates formed were filtered, carefully washed with cold water to get rid of inorganic traces, and recrystallized through methanol or ethanol. The advancement of the reaction and purity during the process were checked using TLC and infrared (IR) spectroscopy.

The separated condensation products were then converted into the desired pyrazole derivatives by cyclizing them with hydrazine and subsequently modifying them with different isocyanates. The changes were made in line with updated literature guidelines [51–53]. During the cyclization phase, the diazo–malononitrile intermediates (**3a** and **3b**) (8 mmol) were refluxed with hydrazine monohydrate (10 mmol) in ethanol (20 mL). To help the ring close, a small amount of piperidine (2–3 drops) was added. After 1–2 h of refluxing, the reaction produced the pyrazole-containing intermediates (see Scheme 1 for compounds **4a** and **4b**). To obtain the final urea-type derivatives, each cyclized intermediate (1 mmol) was combined with the appropriate isocyanate (1.1 mmol) in acetonitrile (5 mL). The reaction mixture had been stirred all night at room temperature. TLC and FT-IR studies were used to ensure that the reaction was complete. After filtering, washing with the right solvents, and recrystallizing, the solid products were ready. All final compounds underwent thorough structural characterization.

4.1.2.1.1 | *3,5-diamino-4-((4-sulfamoylphenyl)diazenyl)-N-(p-tolyl)-1H-pyrazole-1-carboxamide (5a).*

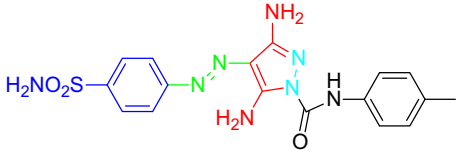

5a

Yield: 72%; Color: light orange; Melting Point: 233°C–234°C; FT-IR (cm^{-1}): 3381, 3322, 3268, 3243 (NH_2), 1701 (C = O), 1615, 1338, 1147 (symmetric) (S = O), 1091; ^1H NMR (DMSO-d_6, 300 MHz, δ ppm): 9.74 (s, 1H, -NH-), 7.95 (d, 2H, $J = 4.2$, Ar-H), 7.84 (d, 2H, $J = 4.2$, Ar-H), 7.68 (d, 2H, $J = 4.2$, Ar-H), 7.38 (s, 2H, -SO_2NH_2), 7.33 (d, 2H, $J = 4.2$, Ar-H), 6.34 (br.s, 2H, -NH_2), 6.10 (br.s, 2H, -NH_2): ^{13}C NMR (DMSO-d_6, 75 MHz, δ ppm): 154.3,

149.5, 139.4, 133.7, 127.5, 126.5, 124.7, 121.2, 120.0, 113.5, 21.6; Anal. Calcd for $C_{17}H_{18}N_8O_3S$ (414.44): C, 49.27; H, 4.38; N, 27.04. Found: C, 49.16; H, 4.25; N, 27.26.

4.1.2.1.2 | 3,5-diamino-N-(4-fluorophenyl)-4-((4-sulfamoylphenyl)diazenyl)-1H-pyrazole-1-carboxamide (5b).

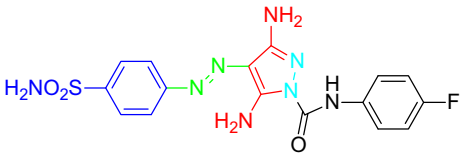

5b

Yield: 72%; Color: light orange; Melting Point: 211°C–213°C; FT-IR (cm^{-1}): 3450, 3404, 3345, 3297 (NH_2), 1701 (C = O), 1618, 1338, 1153 (symmetric) (S = O), 1091; ^1H NMR (DMSO-d_6, 300 MHz, δ ppm): 9.72 (s, 1H, -NH-), 7.97 (d, 2H, J = 4.2, Ar-H), 7.89 (d, 2H, J = 4.2, Ar-H), 7.70 (q, 2H, Ar-H), 7.39 (s, 2H, $-SO_2NH_2$), 7.21 (t, 2H, Ar-H), 6.35 (br.s, 2H, $-NH_2$), 6.10 (br.s, 2H, $-NH_2$): ^{13}C NMR (DMSO-d_6, 75 MHz, δ ppm): 159.9, 158.3, 155.5, 150.74, 142.8, 134.1, 127.1, 123.0, 121.6, 115.7 (d, J = 144), 115.0; Anal. Calcd for $C_{16}H_{15}FN_8O_3S$ (418.41): C, 45.93; H, 3.61; N, 26.78. Found: C, 45.96; H, 3.55; N, 26.81.

4.1.2.1.3 | 3,5-diamino-N-(4-chlorophenyl)-4-((4-sulfamoylphenyl)diazenyl)-1H-pyrazole-1-carboxamide (5c).

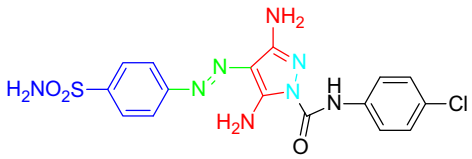

5c

Yield: 68%; Color: light orange; Melting Point: 222°C–224°C; FT-IR (cm^{-1}): 3392, 3359, 3278, 3260 (NH_2), 1703 (C = O), 1617, 1336, 1148 (symmetric) (S = O), 1093; ^1H NMR (DMSO-d_6, 300 MHz, δ ppm): 9.79 (s, 1H, -NH-), 7.96 (d, 2H, J = 4.2, Ar-H), 7.88 (d, 2H, J = 4.2, Ar-H), 7.73 (d, 2H, J = 4.5, Ar-H), 7.42 (d, 2H, J = 4.5, Ar-H), 7.38 (s, 2H, $-SO_2NH_2$), 6.42 (br.s, 2H, $-NH_2$), 6.11 (br.s, 2H, $-NH_2$): ^{13}C NMR (DMSO-d_6, 75 MHz, δ ppm): 154.4, 149.5, 141.7, 135.8, 128.0, 127.2, 126.0, 121.58, 120.4, 114.0; Anal. Calcd for $C_{16}H_{15}ClN_8O_3S$ (434.86): C, 44.19; H, 3.48; N, 25.77. Found: C, 44.16; H, 3.41; N, 25.85.

4.1.2.1.4 | 3,5-diamino-4-((4-sulfamoylphenyl)diazenyl)-N-(m-tolyl)-1H-pyrazole-1-carboxamide (5d).

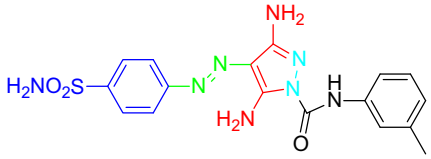

5d

Yield: 79%; Color: light orange; Melting Point: 202°C–203°C; FT-IR (cm^{-1}): 3409, 3363, 3287, 3256 (NH_2), 1691 (C = O), 1622, 1318, 1160 (symmetric) (S = O), 1090; ^1H NMR (DMSO-d_6, 300 MHz, δ ppm): 9.46 (s, 1H, -NH-), 7.97 (d, 2H, J = 4.2, Ar-H), 7.87 (d, 2H, J = 4.2, Ar-H), 7.53 (s, 1H, Ar-H), 7.43 (d, 1H, J = 4.2, Ar-H), 7.38 (s, 2H, $-SO_2NH_2$), 7.24 (t, 1H, Ar-H), 6.95 (d, 1H, J = 4.2, Ar-H), 6.47 (br.s, 2H, $-NH_2$), 6.10 (br.s, 2H, $-NH_2$), 2.31 (s, 3H, $-CH_3$): ^{13}C NMR (DMSO-d_6, 75 MHz, δ ppm): 155.5, 150.5, 142.7, 138.5, 137.6, 129.1, 127.08, 125.2, 121.6, 117.9, 115.0, 21.6; Anal. Calcd for $C_{17}H_{18}N_8O_3S$ (414.44): C, 49.27; H, 4.38; N, 27.04. Found: C, 49.20; H, 4.28; N, 27.18.

4.1.2.1.5 | 3,5-diamino-N-(3-chlorophenyl)-4-((4-sulfamoylphenyl)diazenyl)-1H-pyrazole-1-carboxamide (5e).

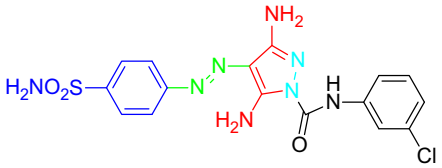

5e

Yield: 73%; Color: light yellow; Melting Point: 218°C–219°C; FT-IR (cm^{-1}): 3465, 3355, 3332, 3281 (NH_2), 1719 (C = O), 1622, 1356, 1151 (symmetric) (S = O), 1090; ^1H NMR (DMSO-d_6, 300 MHz, δ ppm): 9.85 (s, 1H, -NH-), 7.97 (d, 2H, J = 4.5, Ar-H), 7.89 (d, 2H, J = 4.2, Ar-H), 7.87 (s, 1H, Ar-H), 7.64 (d, 1H, J = 4.2, Ar-H), 7.38 (s, 2H, $-SO_2NH_2$), 7.18 (d, 1H, J = 4.5, Ar-H), 6.42 (br.s, 2H, $-NH_2$), 6.12 (br.s, 2H, $-NH_2$): ^{13}C NMR (DMSO-d_6, 75 MHz, δ ppm): 155.5, 150.6, 142.8, 139.5, 133.5, 130.8, 127.1, 124.1, 121.5, 120.4, 119.4, 115.0; Anal. Calcd for $C_{16}H_{15}ClN_8O_3S$ (434.86): C, 44.19; H, 3.48; N, 25.77. Found: C, 44.12; H, 3.39; N, 25.86.

4.1.2.1.6 | 3,5-diamino-N-(3,4-dichlorophenyl)-4-((4-sulfamoylphenyl)diazenyl)-1H-pyrazole-1-carboxamide (5f).

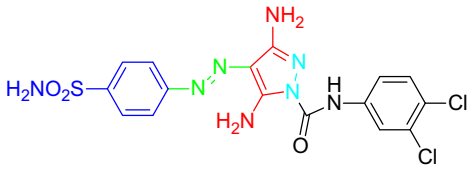

5f

Yield: 76%; Color: light orange; Melting Point: 208°C–210°C; FT-IR (cm^{-1}): 3397, 3388, 3284, 3246 (NH_2), 1705 (C = O), 1617, 1378, 1155 (symmetric) (S = O), 1091; ^1H NMR (DMSO-d_6, 300 MHz, δ ppm): 10.01 (s, 1H, -NH-), 8.10 (s, 1H, Ar-H), 7.97 (d, 2H, J = 4.5, Ar-H), 7.88 (d, 2H, J = 4.5, Ar-H), 7.71 (d, 1H, J = 4.2, Ar-H), 7.62 (d, 1H, J = 4.2, Ar-H), 7.38 (s, 2H, $-SO_2NH_2$), 6.39 (br.s, 2H, $-NH_2$), 6.10 (br.s, 2H, $-NH_2$): ^{13}C NMR (DMSO-d_6, 75 MHz, δ ppm): 155.5, 150.6, 142.8, 138.3, 131.4, 131.0, 127.1, 126.0, 122.2, 121.5, 121.1, 115.0; Anal. Calcd for $C_{16}H_{14}Cl_2N_8O_3S$ (469.31): C, 40.95; H, 3.01; N, 23.88. Found: C, 40.90; H, 3.05; N, 23.92.

4.1.2.1.7 | 3,5-diamino-4-((3-sulfamoylphenyl)diazenyl)-N-(p-tolyl)-1H-pyrazole-1-carboxamide (6a).

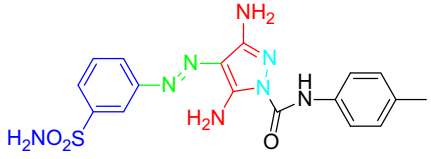

6a

Yield: 86%; Color: light yellow; Melting Point: 228°C–230°C; FT-IR (cm^{-1}): 3439, 3409, 3348, 3290 (NH_2), 1707 (C = O), 1615, 1351, 1160 (symmetric) (S = O), 1086; ^1H NMR (DMSO-d_6, 300 MHz, δ ppm): 9.42 (s, 1H, -NH-), 8.22 (s, 1H, Ar-H), 8.03 (d, 1H, J = 4.2, Ar-H), 7.74 (d, 1H, J = 4.2, Ar-H), 7.63 (t, 1H, Ar-H), 7.54 (d, 2H, J = 4.5, Ar-H), 7.40 (s, 2H, $-SO_2NH_2$), 7.17 (d, 2H,

$J = 4.5$, Ar-H), 6.30 (br.s, 2H, -NH_2), 6.14 (br.s, 2H, -NH_2), 2.28 (s, 3H, -CH_3): ^{13}C NMR (DMSO-d_6, 75 MHz, δ ppm): 153.7, 150.5, 145.6, 135.2, 133.6, 130.0, 129.6, 124.8, 123.8, 120.9, 119.0, 114.6, 20.9; Anal. Calcd for $C_{17}H_{18}N_8O_3S$ (414.44): C, 49.27; H, 4.38; N, 27.04. Found: C, 49.22; H, 4.27; N, 27.16.

4.1.2.1.8 | 3,5-diamino-N-(4-fluorophenyl)-4-((3-sulfamoylphenyl)diazenyl)-1H-pyrazole-1-carboxamide (6b).

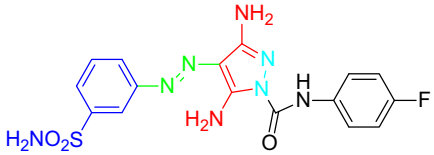

6b

Yield: 89%; Color: light yellow; Melting Point: 199°C–200°C; FT-IR (cm^{-1}): 3456, 3372, 3346, 3311 (NH_2), 1703 (C = O), 1614, 1347, 1163 (symmetric) (S = O), 1089; ^{1}H NMR (DMSO-d_6, 300 MHz, δ ppm): 9.70 (s, 1H, -NH-), 8.22 (s, 1H, Ar-H), 8.03 (d, 1H, $J = 4.2$, Ar-H), 7.74 (d, 1H, $J = 4.2$, Ar-H), 7.70 (q, 1H, Ar-H), 7.63 (d, 2H, $J = 4.2$, Ar-H), 7.40 (s, 2H, -SO_2NH_2), 7.21 (t, 2H, Ar-H), 6.38 (br.s, 2H, -NH_2), 6.15 (br.s, 2H, -NH_2): ^{13}C NMR (DMSO-d_6, 75 MHz, δ ppm): 159.9, 158.3, 153.7, 150.8, 145.6, 134.2, 130.0, 124.8, 123.8, 123.1, 119.1, 115.8 (d, $J = 45$), 114.6; Anal. Calcd for $C_{16}H_{15}FN_8O_3S$ (418.41): C, 45.93; H, 3.61; N, 26.78. Found: C, 45.87; H, 3.56; N, 26.84.

4.1.2.1.9 | 3,5-diamino-N-(4-chlorophenyl)-4-((3-sulfamoylphenyl)diazenyl)-1H-pyrazole-1-carboxamide (6c).

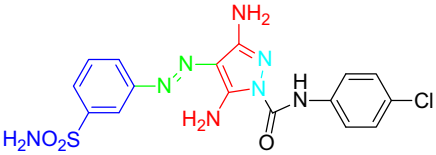

6c

Yield: 72%; Color: light yellow; Melting Point: 206°C–207°C; FT-IR (cm^{-1}): 3426, 3365, 3332, 3309 (NH_2), 1705 (C = O), 1617, 1344, 1151 (symmetric) (S = O), 1089; ^{1}H NMR (DMSO-d_6, 300 MHz, δ ppm): 8.86 (s, 1H, -NH-), 8.11 (s, 1H, Ar-H), 7.89 (d, 1H, $J = 4.2$, Ar-H), 7.64 (d, 1H, $J = 4.2$, Ar-H), 7.56 (t, 1H, Ar-H), 7.49 (d, 2H, $J = 4.5$, Ar-H), 7.31–7.35 (m, 3H, Ar-H ve -SO_2NH_2), 6.40 (br.s, 2H, -NH_2), 5.99 (br.s, 2H, -NH_2): ^{13}C NMR (DMSO-d_6, 75 MHz, δ ppm): 154.4, 152.6, 145.4, 139.0, 129.8, 129.1, 126.0, 123.9, 123.3, 120.3, 118.0, 115.5; Anal. Calcd for $C_{16}H_{15}ClN_8O_3S$ (434.86): C, 44.19; H, 3.48; N, 25.77. Found: C, 44.23; H, 3.42 N, 25.86.

4.1.2.1.10 | 3,5-diamino-4-((3-sulfamoylphenyl)diazenyl)-N-(m-tolyl)-1H-pyrazole-1-carboxamide (6d).

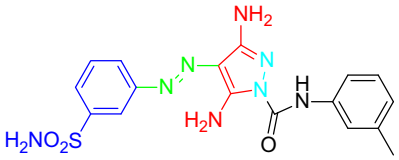

6d

Yield: 74%; Color: light yellow; Melting Point: 189°C–191°C; FT-IR (cm^{-1}): 3422, 3358, 3328, 3301 (NH_2), 1712 (C = O), 1614, 1348, 1161 (symmetric) (S = O), 1086; ^{1}H NMR (DMSO-d_6, 300 MHz, δ ppm): 9.45 (s, 1H, -NH-), 8.24 (s, 1H, Ar-H), 8.04 (d, 1H, $J = 4.2$, Ar-H), 7.75 (d, 1H, $J = 4.2$, Ar-H), 7.64 (t, 1H, Ar-H), 7.53 (s, 1H, Ar-H), 7.44 (d, 1H, $J = 4.2$, Ar-H), 7.41 (s, 2H, -SO_2NH_2), 7.24 (s, 1H, Ar-H), 6.95 (d, 1H, $J = 4.2$, Ar-H), 6.33 (br.s, 2H, -NH_2), 6.15 (br.s, 2H, -NH_2), 2.31 (s, 3H, -CH_3): ^{13}C NMR (DMSO-d_6, 75 MHz, δ ppm): 152.6, 149.4, 144.5, 137.5, 136.5, 129.6, 129.0, 124.8, 123.8, 120.9, 119.0, 114.6, 20.9; Anal. Calcd for $C_{17}H_{18}N_8O_3S$ (414.44): C, 49.27; H, 4.38; N, 27.04. Found: C, 49.23; H, 4.31; N, 27.15.

4.1.2.1.11 | 3,5-diamino-N-(3-chlorophenyl)-4-((3-sulfamoylphenyl)diazenyl)-1H-pyrazole-1-carboxamide (6e).

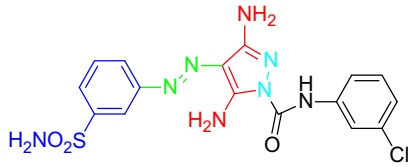

6e

Yield: 72%; Color: light yellow; Melting Point: 198°C–199°C; FT-IR (cm^{-1}): 3436, 3375, 3342, 3295 (NH_2), 1707 (C = O), 1618, 1345, 1160 (symmetric) (S = O), 1088; ^{1}H NMR (DMSO-d_6, 300 MHz, δ ppm): 9.56 (s, 1H, -NH-), 8.22 (s, 1H, Ar-H), 8.06 (d, 1H, $J = 4.2$, Ar-H), 7.78 (d, 1H, $J = 4.2$, Ar-H), 7.69 (t, 1H, Ar-H), 7.51 (s, 1H, Ar-H), 7.48 (d, 1H, $J = 4.2$, Ar-H), 7.40 (s, 2H, -SO_2NH_2), 7.26 (s, 1H, Ar-H), 7.01 (d, 1H, $J = 4.2$, Ar-H), 6.38 (br.s, 2H, -NH_2), 6.12 (br.s, 2H, -NH_2): ^{13}C NMR (DMSO-d_6, 75 MHz, δ ppm): 155.5, 150.4, 144.6, 138.3, 136.4, 130.1, 128.7, 125.7, 123.4, 121.1, 119.2, 115.3; Anal. Calcd for $C_{16}H_{15}ClN_8O_3S$ (434.86): C, 44.19; H, 3.48; N, 25.77. Found: C, 44.11; H, 3.41; N, 25.88.

4.1.2.1.12 | 3,5-diamino-N-(3,4-dichlorophenyl)-4-((3-sulfamoylphenyl)diazenyl)-1H-pyrazole-1-carboxamide (6f).

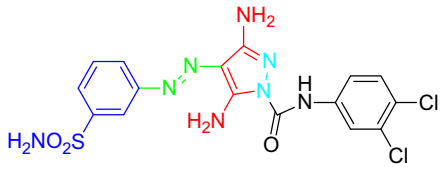

6f

Yield: 78%; Color: light yellow; Melting Point: 193°C–195°C; FT-IR (cm^{-1}): 3442, 3350, 3338, 3278 (NH_2), 1710 (C = O), 1630, 1348, 1162 (symmetric) (S = O), 1089; ^{1}H NMR (DMSO-d_6, 300 MHz, δ ppm): 10.01 (s, 1H, -NH-), 8.24 (s, 1H, Ar-H), 8.09 (s, 1H, Ar-H), 8.04 (d, 1H, $J = 3.9$, Ar-H), 7.75 (d, 1H, $J = 3.9$, Ar-H), 7.71 (d, 1H, $J = 3.9$, Ar-H), 7.60–7.65 (m, 2H, Ar-H), 7.41 (s, 2H, -SO_2NH_2), 6.38 (br.s, 2H, -NH_2), 6.20 (br.s, 2H, -NH_2): ^{13}C NMR (DMSO-d_6, 75 MHz, δ ppm): 151.5, 148.5, 143.5, 136.1, 129.3, 128.8, 127.9, 123.9, 122.7, 121.7, 120.1, 118.9, 117.1, 112.4; Anal. Calcd for $C_{16}H_{14}Cl_2N_8O_3S$ (469.31): C, 40.95; H, 3.01; N, 23.88. Found: C, 40.89; H, 3.08; N, 23.95.

4.2 | CA Inhibition

To evaluate the catalytic/inhibitory activity of different CA isozymes, an SX.18 MV-R Applied Photophysics (Oxford, UK) stopped-flow instrument was used [60]. We used Phenol Red as an indicator at a concentration of 0.2 mM and an absorbance peak of 557 nm. The buffer solution contained 10 mM Hepes (pH 7.4) and 0.1 M Na_2SO_4 or $NaClO_4$ to maintain a stable ionic strength. At this concentration, these anions did not stop the reaction. For 5–10 s, the CA-catalyzed CO_2 hydration reaction was watched. We used saturated CO_2 solutions in water at 25°C as substrates.

We made stock solutions of inhibitors at 10 mM (in DMSO-water 1:1, v/v) and then diluted them to 0.01 nM in the assay buffer we have previously discussed. Before the assay, the inhibitor and enzyme solutions were mixed together and left at room temperature for 10 min to form the E–I complex. To determine the inhibition constant, at least 7 different inhibitor concentrations were used. We tested each inhibitor concentration three times, and the numbers you see here are the averages of those three tests. We used the Cheng–Prusoff equation and nonlinear least-squares methods to estimate the inhibition constants, which were averaged across at least 3 separate tests. The CA isozymes employed in this study were recombinant proteins previously acquired by our research group [18, 61–66].

4.3 | Cytotoxic Activity Analysis of Test Compounds

4.3.1 | Cell Lines and Culture

In cytotoxic activity experiments, the human nonsmall cell lung cancer cell line (A549) and the human colorectal carcinoma cell line (HCT116), obtained from the American Type Culture Collection (ATCC), were used. Cells were cultured in RPMI-1640 cell culture medium containing 10% fetal bovine serum (FBS) and 1% penicillin/streptomycin and maintained in a CO_2 incubator at 37°C.

4.3.2 | MTT Cell Viability Analysis

For the study, cells were plated at a density of 6×10^5 cells/mL. When the cells reached 80% confluence, they were exposed to test compounds prepared at concentrations of 120, 60, 30, 15, 7.5, and 3.75 μM for 24 h. All test compounds were dissolved in DMSO, and the highest DMSO concentration was used as a negative control. In this study, Cisplatin (dissolved in PBS) and SLC-0111 (dissolved in DMSO) were included as reference compounds for comparative evaluation rather than as positive controls. The MTT (3-[4,5-dimethylthiazol-2-yl]−2,5-diphenyl tetrazolium bromide) test was used to assess cell viability. In this test, MTT is reduced to formazan via cellular enzymatic reactions, forming insoluble particles that are later dissolved in DMSO. The prepared MTT solution (1 mg/mL) was added to the cells, which were incubated at 37°C for 45 min. Subsequently, absorbance was measured at 550 nm using a microplate spectrophotometer.

4.4 | Molecular Docking Analysis

The high-resolution X-ray crystal structures of hCA IX (PDB ID: 5FL4) [67] and XII (PDB ID: 8CO3) [68] were retrieved from the Protein Data Bank. Prior to docking simulations, the receptor structures were meticulously prepared to ensure accurate binding environment representation [69]. This preparation involved the removal of all water molecules, native co-crystallized ligands, and nonessential heteroatoms. Crucially, for the hCA IX model (5FL4), the co-crystallized glycerol molecule (Gol 271) was explicitly deleted; as a recognized cryoprotectant crystallization artifact, its removal was strictly necessary to prevent artefactual hydrogen bonding and the subsequent skewing of calculated binding affinities. Following the purification of the coordinate files, polar hydrogens were added, and standard atomic charges were assigned to generate the final receptor models.

Simultaneously, the 3D structures of the synthesized pyrazole derivatives (**5d**, **5e**, **5f**) and the reference inhibitor acetazolamide (AAZ) were constructed, subjected to geometry optimization, and prepared with fully assigned rotatable bonds. Molecular docking experiments were subsequently executed utilizing AutoDock Vina [69, 70]. To facilitate targeted docking, the search space was defined by generating grid boxes strictly centered around the catalytic zinc ion of each isoform ($x = 7.167$; $y = -25.410$; $z = 57.347$, and $X = 0.033$; $y = 0.456$; $z = 4.186$ for hCA IX and hCA XII, respectively). These grid dimensions were calibrated to encompass the conserved histidine coordination triad alongside the adjacent active site cleft, thereby allowing for comprehensive conformational sampling of the extended pyrazole scaffolds. The grid box volumes were set to be 22 Å × 22 Å × 22 Å. pH and exhaustiveness were set to be 7.4 and 20, respectively.

Following the docking runs, the generated ligand conformations were ranked according to their predicted binding free energies. The optimal, lowest-energy binding poses were extracted and subjected to rigorous post-docking structural analysis using the PyMOL Molecular Graphics System, version 3.0.0. PyMOL 3.0.0 [71] was specifically employed to render the 3D binding geometries, visually validate the primary metal-acceptor coordination with the catalytic zinc, and map the complex networks of hydrogen bonding, π–π stacking, and hydrophobic contacts driving the interactions within the active sites of both hCA IX and hCA XII.

Author Contributions

Suleyman Akocak: conceptualization, methodology, data curation, investigation, validation, formal analysis, supervision, funding acquisition, writing – review & editing, writing – original draft. **Nebih Lolak:** methodology, data curation, investigation, validation. andrea ammara: data curation, validation, formal analysis. **Gökçenur Gürbüz:** methodology, data curation, validation. **Ibrahim Bozgeyik:** methodology, data curation, validation. **Demet Taşdemir:** methodology, data curation, validation, formal analysis. **Hamada Hashem:** software, data curation, validation, visualization. **Stefan Bräse:** software, data curation, visualization, writing – review & editing. **Claudiu T. Supuran:** methodology, supervision, writing – original draft, writing – review & editing, validation.

Acknowledgments

This work was supported by TUBITAK (The Scientific and Technological Research Council of Turkey) for a research grant (Project No: 223Z179). Also, this study partially supported by the Research Fund of Adıyaman University (grant number ECZMAP/2023–0002).

Funding

This study was supported by Türkiye Bilimsel ve Teknolojik Araştırma Kurumu (223Z179).

Conflicts of Interest

The authors declare no conflicts of interest.

Data Availability Statement

Data will be made available on request.

References

1. C. T. Supuran, "Carbonic Anhydrases: Novel Therapeutic Applications for Inhibitors and Activators," *Nature Reviews Drug Discovery* 7 (2008): 168–181.

2. C. T. Supuran, "How Many Carbonic Anhydrase Inhibition Mechanisms Exist?," *Journal of Enzyme Inhibition and Medicinal Chemistry* 31 (2015): 345–360.

3. K. D'Ambrosio, A. Di Fiore, V. Alterio, et al., "Multiple Binding Modes of Inhibitors to Human Carbonic Anhydrases: An Update on the Design of Isoform-Specific Modulators of Activity," *Chemical Reviews* 125 (2025): 150–222.

4. C. T. Supuran, "Multi- and Polypharmacology of Carbonic Anhydrase Inhibitors," *Pharmacological Reviews* 77 (2025): 100004.

5. A. B. Vermelho, G. C. Rodrigues, A. Nocentini, F. R. Mansoldo, and C. T. Supuran, "Discovery of Novel Drugs for Chagas Disease: Is Carbonic Anhydrase a Target for Antiprotozoal Drugs?," *Expert Opinion on Drug Discovery* 17 (2022): 1147–1158.

6. S. Giovannuzzi, C. T. Supuran, "Human Carbonic Anhydrase Modulators: the past, Present, and Future," *Trends in pharmacological sciences* 46 (2025): 836.

7. S. Akocak and C. T. Supuran, "Activation of α-, β-, γ- δ-, ζ- and η- Class of Carbonic Anhydrases with Amines and Amino Acids: A Review," *Journal of Enzyme Inhibition and Medicinal Chemistry* 34 (2019): 1652–1659.

8. C. T. Supuran, "A Simple yet multifaceted 90 years Old, Evergreen Enzyme: Carbonic Anhydrase, Its Inhibition and Activation," *Bioorganic & Medicinal Chemistry Letters* 93 (2023): 129411.

9. D. Neri and C. T. Supuran, "Interfering with pH Regulation in Tumours as a Therapeutic Strategy," *Nature Reviews Drug Discovery* 10 (2011): 767–777.

10. S. Akocak, M. R. Alam, A. M. Shabana, et al., "PEGylated Bis-Sulfonamide Carbonic Anhydrase Inhibitors Can Efficiently Control the Growth of Several Carbonic Anhydrase IX-Expressing Carcinomas," *Journal of Medicinal Chemistry* 59 (2016): 5077–5088.

11. T. Tekeli, S. Akocak, A. Petreni, N. Lolak, S. Çete, and C. T. Supuran, "Potent Carbonic Anhydrase I, II, IX and XII Inhibition Activity of Novel Primary Benzenesulfonamides Incorporating Bis-Ureido Moieties," *Journal of Enzyme Inhibition and Medicinal Chemistry* 38 (2023): 2185762.

12. H. Küçükbay, Z. Gönül, F. C. Z. Küçükbay, et al., "Synthesis of New 7-amino-3,4-dihydroquinolin-2(1 *H*)-one-peptide Derivatives and Their Carbonic Anhydrase Enzyme Inhibition, Antioxidant, and Cytotoxic Activities," *Archiv der Pharmazie* 354 (2021): 2100122.

13. A. Aspatwar, M. E. E. Tolvanen, H. Barker, et al., "Carbonic Anhydrases in Metazoan Model Organisms: Molecules, Mechanisms, and Physiology," *Physiological Reviews* 102 (2022): 1327–1383.

14. A. García-Llorca, F. Carta, C. T. Supuran, and T. Eysteinsson, "Carbonic Anhydrase, Its Inhibitors and Vascular Function," *Frontiers in Molecular Biosciences* 11 (2024): 1338528.

15. F. Fiorentino, A. Nocentini, D. Rotili, C. T. Supuran, and A. Mai, "Antihistamines, Phenothiazine-Based Antipsychotics, and Tricyclic Antidepressants Potently Activate Pharmacologically Relevant Human Carbonic Anhydrase Isoforms II and VII," *Journal of Enzyme Inhibition and Medicinal Chemistry* 38 (2023): 2188147.

16. S. Deniz, T. K. Uysal, C. Capasso, C. T. Supuran, and O. Ozensoy Guler, "Is Carbonic Anhydrase Inhibition Useful as a Complementary Therapy of Covid-19 Infection?," *Journal of Enzyme Inhibition and Medicinal Chemistry* 36 (2021): 1230–1235.

17. O. Ozensoy Guler, C. T. Supuran, and C. Capasso, "Carbonic Anhydrase IX as a Novel Candidate in Liquid Biopsy," *Journal of Enzyme Inhibition and Medicinal Chemistry* 35 (2020): 255–260.

18. W. M. Eldehna, M. Fares, A. Bonardi, et al., "4-(Pyrazolyl)benzene-sulfonamide Ureas as Carbonic Anhydrases Inhibitors and Hypoxia-Mediated Chemo-Sensitizing Agents in Colorectal Cancer Cells," *Journal of Medicinal Chemistry* 67 (2024): 20438–20454.

19. J. Leinonen and S. Parkkila, *Carbonic Anhydrases as Biocatalysts*, (Elsevier, 2015), 139–149.

20. A. Aspatwar, L. Syrjänen, and S. Parkkila, "Roles of Carbonic Anhydrases and Carbonic Anhydrase Related Proteins in Zebrafish," *International Journal of Molecular Sciences* 23 (2022): 4342.

21. R. Ronca and C. T. Supuran, "Carbonic anhydrase IX: An atypical target for innovative therapies in cancer," *Biochimica et Biophysica Acta (BBA) - Reviews on Cancer* 1879 (2024): 189120.

22. A. E. Elsawi, M. M. Elbadawi, A. Nocentini, et al., "1,5-Diaryl-1,2,4-Triazole Ureas as New SLC-0111 Analogues Endowed with Dual Carbonic Anhydrase and VEGFR-2 Inhibitory Activities," *Journal of Medicinal Chemistry* 66 (2023): 10558–10578.

23. S. Akocak and M. A. Ilies, "Next-generation primary sulfonamide carbonic anhydrase inhibitors," in *Targeting Carbonic Anhydrases*, (Future Science, 2014), 35–51.

24. S. Singh, C. L. Lomelino, M. Y. Mboge, S. C. Frost, and R. McKenna, "Cancer Drug Development of Carbonic Anhydrase Inhibitors beyond the Active Site," *Molecules* 23 (2018): 1045.

25. C. T. Supuran, "Targeting carbonic anhydrases for the management of hypoxic metastatic tumors," *Expert Opinion on Therapeutic Patents* 33 (2023): 701–720.

26. C. T. Supuran, "Emerging Role of Carbonic Anhydrase Inhibitors," *Clinical Science* 135 (2021): 1233–1249.

27. C. Li, G. Zhang, L. Zhao, Z. Ma, and H. Chen, "Metabolic Reprogramming in Cancer Cells: Glycolysis, Glutaminolysis, and Bcl-2 Proteins as Novel Therapeutic Targets for Cancer," *World Journal of Surgical Oncology* 14 (2015): 15.

28. M. Benej, S. Pastorekova, and J. Pastorek, *Carbonic Anhydrase*, (Springer Netherlands, 2013), 199–219.

29. S. H. Lee and J. R. Griffiths, "How and Why Are Cancers Acidic? Carbonic Anhydrase IX and the Homeostatic Control of Tumour Extracellular pH," *Cancers* 12 (2020): 1616.

30. S. Habib, R. Tabassum, Z. A. Shahid, M. S. Ashraf, and K. Fayyaz, "Synthesis of heterocyclic Diazenyl derivatives and their metal complexes: Exploring antioxidant, antimicrobial potential and in silico targeting of diabetes related," *Polyhedron* 283 (2025): 117814.

31. S. Akocak, N. Lolak, S. Giovannuzzi, and C. T. Supuran, "Potent and Selective Carbonic Anhydrase Inhibition Activities of Pyrazolones

Bearing Benzenesulfonamides," *Bioorganic & Medicinal Chemistry Letters* 95 (2023): 129479.

32. D. Kölmel, N. Jung, and S. Bräse, "Azides – Diazonium Ions – Triazenes: Versatile Nitrogen-Rich Functional Groups," *Australian Journal of Chemistry* 67 (2014): 328–336.

33. N. Lolak, S. Akocak, M. Topal, et al., "Sulfonamide-Bearing Pyrazolone Derivatives as Multitarget Therapeutic Agents: Design, Synthesis, Characterization, Biological Evaluation, In Silico ADME /T Profiling and Molecular Docking Study," *Pharmacology Research & Perspectives* 13 (2025): e70088.

34. F. Marchesi, M. Turriziani, G. Tortorelli, G. Avvisati, F. Torino, and L. De Vecchis, "Triazene Compounds: Mechanism of Action and Related DNA Repair Systems," *Pharmacological Research* 56 (2007): 275–287.

35. Z. R. Al-Majdi, W. H. Al-Dahhan, M. S. Shihab, and M. H. Nazari, "Azo Compounds and Their Potential Applications: Article Review," *Al-Kitab Journal for Pure Sciences* 9 (2024): 144–163.

36. T. Tahir, M. Ashfaq, M. Saleem, et al., "Pyridine Scaffolds, Phenols and Derivatives of Azo Moiety: Current Therapeutic Perspectives," *Molecules* 26 (2021): 4872.

37. K. Mezgebe and E. Mulugeta, "Synthesis and Pharmacological Activities of Azo Dye Derivatives Incorporating Heterocyclic Scaffolds: A Review," *RSC Advances* 12 (2022): 25932–25946.

38. M. Lusardi, A. Spallarossa, and C. Brullo, "Amino-Pyrazoles in Medicinal Chemistry: A Review," *International Journal of Molecular Sciences* 24 (2023): 7834.

39. M. Marinozzi, G. Marcelli, and A. Carotti, "N-Aryl-5-Aminopyrazole: A Versatile Architecture in Medicinal Chemistry," *Mini Reviews in Medicinal Chemistry* 15 (2015): 272–299.

40. K. Karrouchi, S. Radi, Y. Ramli, et al., "Synthesis and Pharmacological Activities of Pyrazole Derivatives: A Review," *Molecules* 23 (2018): 134.

41. D. M. Odeh, M. M. Odeh, T. S. Hafez, and A. S. Hassan, "Bioactive Fused Pyrazoles Inspired by the Adaptability of 5-Aminopyrazole Derivatives: Recent Review," *Molecules* 30 (2025): 366.

42. A. Fekri, E. M. Keshk, A. G. M. Khalil, and I. Taha, "Synthesis of Novel Antioxidant and Antitumor 5-Aminopyrazole Derivatives, 2D/3D QSAR, and Molecular Docking," *Molecular Diversity* 26 (2022): 781–800.

43. A. A. Hamad, E. K. M. Zangana, R. A. Omer, et al., "Design, Synthesis of Novel Pyrazole Derivatives and Demonstrate their Biological Activity as Drug Candidates: A Review," *Chemical Review and Letters* 8 (2025): 867–882.

44. R. Jorda, E. Schuetznerova, P. Cankař, V. Brychtová, J. Navratilova, and V. Kryštof, "Novel Arylazopyrazole Inhibitors of Cyclin-Dependent Kinases," *Bioorganic & Medicinal Chemistry* 23 (2015): 1975–1981.

45. M. A. Said, W. M. Eldehna, A. Nocentini, et al., "Sulfonamide-Based ring-Fused Analogues for CAN508 as Novel Carbonic Anhydrase Inhibitors Endowed with Antitumor Activity: Design, Synthesis, and in vitro Biological Evaluation," *European Journal of Medicinal Chemistry* 189 (2020): 112019.

46. V. Krystof and S. Uldrijan, "Cyclin-Dependent Kinase Inhibitors as Anticancer Drugs," *Current Drug Targets* 11 (2010): 291–302.

47. V. Kryštof, P. Cankař, I. Fryšová, et al., "4-Arylazo-3,5-Diamino-1 *H* -Pyrazole CDK Inhibitors: SAR Study, Crystal Structure in Complex with CDK2, Selectivity, and Cellular Effects," *Journal of Medicinal Chemistry* 49 (2006): 6500–6509.

48. K. E. Anwer, N. M. El-Dydamony, A. Saleh, N. Altwaijry, and E. M. Husseiny, "Comparative Study of Conventional, Grinding, and Microwave-Assisted Synthesis of Aminopyrazolones and Diamino-pyrazoles: Exploring the Antitumor Activity, Dual CDK-2/CA IX Inhibition Potential, and Apoptosis Induction," *Drug Development Research* 86 (2025): e70139.

49. S. Bräse, *Privileged Scaffolds in Medicinal Chemistry: Design, Synthesis and Evaluation*, (RSC Publishing, 2015).

50. Z. Gao, W. Huang, M. Liu, et al., "Highly Efficient Construction of Multi-Substituted Aminopyrazoles Derivatives *via* Iodine-Mediated Three-Components Reaction as Potential Anticancer Agents," *Green Chemistry Letters and Reviews* 16 (2023): 2264324.

51. S. Akocak, N. Lolak, A. Ammara, Ö.Ö. Güler, and C. T. Supuran, "Exploring the Carbonic Anhydrase Activation Properties of 4-arylazo-3, 5-diamino-1H-pyrazoles against hCA I, II, IV, and VII isoenzymes," *Current Topics in Medicinal Chemistry* 25 (2025): 3281.

52. G. Yapar, N. Lolak, A. Bonardi, S. Akocak, and C. T. Supuran, "Exploring the Potency of Diazo-coumarin Containing Hybrid Molecules: Selective Inhibition of Tumor-associated Carbonic Anhydrase Isoforms IX and XII," *ChemMedChem* 19 (2024): e202300626.

53. M. Durgun, S. Akocak, N. Lolak, et al., "Design and Synthesis of Pyrazole Carboxamide Derivatives as Selective Cholinesterase and Carbonic Anhydrase Inhibitors: Molecular Docking and Biological Evaluation," *Chemistry & Biodiversity* 21 (2024): e202301824.

54. E. J.Schütznerová, I. Popa, V. Kryštof, et al., "Utilization of DmbNHNH2 in the Synthesis of Amino-Substituted 4-((3,5-Diamino-1H-Pyrazol-4-Yl)diazenyl)phenols," *Tetrahedron* 68 (2012): 3996–4002.

55. E. M. Husseiny, H. S. Abulkhair, N. M. El-Dydamony, K. E. Anwer, "Exploring the Cytotoxic Effect and CDK-9 Inhibition Potential of Novel Sulfaguanidine-Based Azopyrazolidine-3, 5-Diones and 3, 5-diaminoazo-pyrazoles," *Bioorganic Chemistry* 133 (2023): 106397.

56. J. C. Castillo and J. Portilla, "Recent advances in the synthesis of new pyrazole derivatives," *Targets in Heterocyclic Systems* 22 (2018): 194–223.

57. S. Maddila, S. B. Jonnalagadda, K. K. Gangu, and S. N. Maddila, "Recent Advances in the Synthesis of Pyrazole Derivatives Using Multicomponent Reactions," *Current Organic Synthesis* 14 (2017): 634–653.

58. I. Ameziane El Hassani, K. Rouzi, H. Assila, K. Karrouchi, and M. Ansar, "Recent Advances in the Synthesis of Pyrazole Derivatives: A Review," *Reactions* 4 (2023): 478–504.

59. R. Ramajayam, "A Comprehensive Review on Traditional and Modern Synthetic Approaches to Pyrazole and Its Analogs," *Journal of Heterocyclic Chemistry* 62 (2025): 1424–1462.

60. R. G. Khalifah, "The Carbon Dioxide Hydration Activity of Carbonic Anhydrase," *Journal of Biological Chemistry* 246 (1971): 2561–2573.

61. W. M. Eldehna, M. Fares, E. Berrino, et al., "SLC-0111 Enaminone Analogs, 3/4-(3-Aryl-3-Oxopropenyl) Aminobenzenesulfonamides, as Novel Selective Subnanomolar Inhibitors of the Tumor-Associated Carbonic Anhydrase Isoform IX," *Bioorganic Chemistry* 83 (2019): 549–558.

62. U. K. Mondal, K. Doroba, A. M. Shabana, et al., "PEG Linker Length Strongly Affects Tumor Cell Killing by PEGylated Carbonic Anhydrase Inhibitors in Hypoxic Carcinomas Expressing Carbonic Anhydrase IX," *International Journal of Molecular Sciences* 22 (2021): 1120.

63. A. M. Shabana, U. K. Mondal, M. R. Alam, et al., "pH-Sensitive Multiligand Gold Nanoplatform Targeting Carbonic Anhydrase IX Enhances the Delivery of Doxorubicin to Hypoxic Tumor Spheroids and Overcomes the Hypoxia-Induced Chemoresistance," *ACS Applied Materials & Interfaces* 10 (2018): 17792–17808.

64. M. Oguz, E. Kalay, S. Akocak, et al., "Synthesis of Calix[4]azacrown Substituted Sulphonamides with Antioxidant, Acetylcholinesterase, Butyrylcholinesterase, Tyrosinase and Carbonic Anhydrase Inhibitory Action," *Journal of Enzyme Inhibition and Medicinal Chemistry* 35 (2020): 1215–1223.

65. S. M. Hefny, T. F. El-Moselhy, N. El-Din, et al., "A New Framework for Novel Analogues of Pazopanib as Potent and Selective Human Carbonic Anhydrase Inhibitors: Design, Repurposing Rational, Synthesis, Crystallographic, In Vivo and In Vitro Biological Assessments," *European Journal of Medicinal Chemistry* 274 (2024): 116527.

66. C. M. Al-Matarneh, M. Pinteala, A. Nicolescu, et al., "Synthetic Approaches to Novel Human Carbonic Anhydrase Isoform Inhibitors Based on Pyrrol-2-One Moiety," *Journal of Medicinal Chemistry* 67 (2024): 3018–3038.

67. J. Leitans, A. Kazaks, A. Balode, et al., "Efficient Expression and Crystallization System of Cancer-Associated Carbonic Anhydrase Isoform IX," *Journal of Medicinal Chemistry* 58 (2015): 9004–9009.

68. J. Ivanova, A. Nocentini, K. Tars, et al., "Atropo/Tropo Flexibility: A Tool for Design and Synthesis of Self-Adaptable Inhibitors of Carbonic Anhydrases and Their Antiproliferative Effect," *Journal of Medicinal Chemistry* 66 (2023): 5703–5718.

69. H. Hashem, S. Abdelfattah, H. M. Hassan, et al., "Discovery of a Novel 4-Pyridyl SLC-0111 Analog Targeting Tumor-Associated Carbonic Anhydrase Isoform IX through Tail-Based Design Approach with Potent Anticancer Activity," *Frontiers in Chemistry* 13 (2025): 1571646.

70. J. Eberhardt, D. Santos-Martins, A. F. Tillack, and S. Forli, "AutoDock Vina 1.2. 0: new docking methods, expanded force field, and python bindings," *Journal of chemical information and modeling* 61 (2021): 3891–3898.

71. S. Yuan, H. C. S. Chan, and Z. Hu, "Using PyMOL as a platform for computational drug design," *Wiley Interdisciplinary Reviews: Computational Molecular Science* 7, no. 2 (2017): e1298.

Supporting Information

Additional supporting information can be found online in the Supporting Information section.